


Article

# Structure and Electrochemical Properties of $\text{Mn}_3\text{O}_4$ Nanocrystal-Coated Porous Carbon Microfiber Derived from Cotton

Dongya Sun <sup>1,2,\*</sup> , Liwen He <sup>1,2</sup>, Yongle Lai <sup>1</sup>, Jiqiong Lian <sup>1</sup>, Jingjing Sun <sup>1</sup>, An Xie <sup>1</sup> and Bizhou Lin <sup>2,\*</sup>

<sup>1</sup> Key Laboratory of Functional Materials and Applications of Fujian Province, School of Materials Science and Engineering, Xiamen University of Technology, Xiamen 361024, China; heliwen@hqu.edu.cn (L.H.); 2013123201@xmut.edu.cn (Y.L.); 2013123202@xmut.edu.cn (J.L.); 2015000093@xmut.edu.cn (J.S.); anxie@xmut.edu.cn (A.X.)

<sup>2</sup> Fujian Key Laboratory of Photoelectric Functional Materials, College of Materials Science and Engineering, Huaqiao University, Xiamen 361021, China

\* Correspondence: 2013123205@xmut.edu.cn (D.S.); bzlinhqu@126.com (B.L.)

Received: 16 September 2018; Accepted: 12 October 2018; Published: 15 October 2018



**Abstract:** Biomorphous  $\text{Mn}_3\text{O}_4$  nanocrystal/porous carbon microfiber composites were hydrothermally fabricated and subsequently calcined using cotton as a biotemplate. The as-prepared material exhibited a specific capacitance of  $140.8 \text{ F} \cdot \text{g}^{-1}$  at  $0.25 \text{ A} \cdot \text{g}^{-1}$  and an excellent cycle stability with a capacitance retention of 90.34% after 5000 cycles at  $1 \text{ A} \cdot \text{g}^{-1}$ . These characteristics were attributed to the introduction of carbon fiber, the high specific surface area, and the optimized microstructure inherited from the biomaterial.

**Keywords:**  $\text{Mn}_3\text{O}_4$ ; carbon microfibers; biotemplate; microstructure; energy storage and conversion; electrochemical properties

## 1. Introduction

Electrochemical supercapacitors (ESs) have many desirable properties, including long lifetime, high power density, and high rate capability. Thus, ESs are attracting worldwide attention as an efficient energy storage device for portable electronic devices and vehicles [1,2]. Transition metal oxides (TMOs) such as  $\text{CoO}_x$ ,  $\text{NiO}$ , and  $\text{MnO}_x$  have been extensively investigated as promising electrode materials for ES applications. These oxides deliver higher specific capacitances than those of carbonaceous materials due to reversible faradaic redox reactions [2]. Manganese oxide has been considered a highly attractive TMO due to its high theoretical specific capacitance, good electrochemical stability, low cost, and natural abundance [3].  $\text{MnO}_x$ -based composites with various microstructures and morphologies, such as wires, sheets, tubes, and flowers, have been developed [4–7]. Although these active materials exhibit enhanced pseudocapacitance properties, their low electronic conductivity and insufficient interface contact can substantially reduce the experimental specific capacitance and hamper their extensive commercial application.

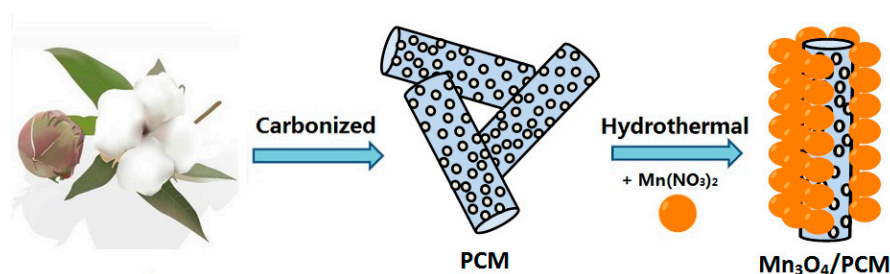
To address these issues, scholars have proposed the fabrication of many  $\text{MnO}_x$ /carbon composites in recent years [8,9]. Among the carbon materials, using low-cost natural resources, biowaste, and food waste are highly effective ways to achieve the large-scale production of electrode materials [10–12]. Natural biomaterials usually possess irregular microstructures that are difficult to duplicate, and these structures are often highly suitable as energy storage materials. For example, cotton wool [6], coconut shell [13], and human hair [14] have been introduced as excellent flexible carbon substrates for hybrid composites. These materials exhibit high specific capacitance, good electronic conductivity,

good cycle stability, and excellent flexibility. Therefore, a simple and cheap approach using porous carbon microfiber (PCM) derived from cotton wool was studied in our work.

Herein, we prepared a biomorphic porous composite fabricated using  $\text{Mn}_3\text{O}_4$  nanocrystals supported on PCMs ( $\text{Mn}_3\text{O}_4/\text{PCM}$ ) with cotton fiber as the biotemplate and carbon skeleton. Benefitting from the unique morphology, large specific surface area, and existence of carbon fiber, the as-prepared composites exhibit an excellent electrochemical performance.

## 2. Experimental

The preparation process of  $\text{Mn}_3\text{O}_4/\text{PCM}$  is schematically illustrated in Scheme 1. Dry cotton wool (Xinghua health cotton wool Co. LTD, Xinghua, China) was cut into short pieces and carbonized for 1 h at 350 °C under an argon atmosphere. The as-prepared sample is denoted as PCM. Then, 2.5 g PCM was immersed in 50 mL of 1 mol·L<sup>-1</sup>  $\text{Mn}(\text{NO}_3)_2 \cdot 6\text{H}_2\text{O}$  solution. The dispersed solution was transferred to a 100 mL autoclave and reacted for 12 h at 180 °C. The hydrothermal reaction product was filtered, washed, dried, and annealed in a tubular furnace at 400 °C in air for 1 h, and the product was labeled as  $\text{Mn}_3\text{O}_4/\text{PCM}$ . For comparison, pristine  $\text{Mn}_3\text{O}_4$  was hydrothermally synthesized by decomposing the solution of  $\text{Mn}(\text{NO}_3)_2 \cdot 6\text{H}_2\text{O}$  at 180 °C for 12 h without cotton.



**Scheme 1.** Illustration of the preparation process of  $\text{Mn}_3\text{O}_4/\text{PCM}$  (porous carbon microfiber).

Field emission scanning electron microscopy (FE-SEM) images were taken with a Zeiss Sigma 500 microscope (Carl Zeiss A G, Jena, German) and an Oxford X-Max energy dispersive spectroscopy (EDS, Oxford instruments, Oxford, UK). Transmission electron microscopy (TEM) images were taken using a FEI Talos F200S microscope (Thermo fisher Scientific, Waltham, MA, USA) with an accelerating voltage of 200 kV. Powder X-ray diffraction (XRD) patterns were obtained at ambient temperature on a Rigaku Smart Lab 3 kW diffractometer (Rigaku, Tokyo, Japan) using Cu K radiation ( $\lambda = 1.5418 \text{ \AA}$ ) under an accelerating voltage of 36 kV. Raman spectroscopy was tested with the range of 300–2000  $\text{cm}^{-1}$  on a LABRAM HR-800 spectrometer (Horiba, Kyoto, Japan), and the excitation source was a 532 nm laser. Specific surface area and porosity measurements were carried out on a Quantachrome Autosorb-iQ instrument (Quantachrome instruments, Boynton Beach, FL, USA) using the Brunauer–Emmett–Teller (BET) method. X-ray photoelectron spectroscopy (XPS) measurements were performed on a VG Escalab MK II spectrometer (Thermo fisher Scientific, Waltham, MA, USA) with non-monochromatic Al K $\alpha$  X-ray (1486.6 eV). The TG-DTA were measured on an integrated thermal analyzer (TG, STA 449C, NETZSCH-Gerätebau GmbH, Selb, Germany) with a 10 °C/min heating rate from room temperature to 750 °C under air atmosphere. The working electrode was prepared by mixing the prepared composites, acetylene black, and polytetrafluoroethylene with a mass ratio of 75:15:10, while electrode of the bulk  $\text{Mn}_3\text{O}_4$  was 50:40:10. The net weight of  $\text{Mn}_3\text{O}_4$  in electrodes was ~3 mg. Subsequently, the mixture was coated onto a nickel foam current collector (1.5  $\text{cm}^2$ ), pressed at 10 MPa, and dried under vacuum at 60 °C. All the measurements were performed with a three-electrode system (Hg/HgO and platinum as the reference and counter electrode, respectively) and a two-electrode system ( $\text{Mn}_3\text{O}_4/\text{PCM}$  and commercial active carbon (CAC)) in 3 mol·L<sup>-1</sup> KOH aqueous electrolyte.

### 3. Results and Discussion

The carbon fiber of the cotton became remarkably porous after carbonization (Figure 1a). The  $\text{Mn}_3\text{O}_4$ /PCM composite prepared using cotton as template had a tubular morphology (Figure 1b,c) similar to cotton. At the start of the hydrothermal reaction, the cotton was immersed into the precursor solution, the  $\text{Mn}^{2+}$  was partly oxidized to  $\text{Mn}^{3+}$  ions, and  $\text{Mn}_3\text{O}_4$  formed. Mn ions were then bonded onto the oxygen-rich group of the cotton fibers through O-H, C=O groups, and so on (Figure 1b) [15–17]. The size of nanocrystals increased from several to dozens of nanometers (Figure 1b,c) with a reaction time from 5 h to 12 h. When the hydrothermal product was calcined at 400 °C, the precise replication of cotton texture could be achieved after the removal of most of the template substance. Part of the organic template was carbonized into a porous carbon stick with irregular pores (Figure 1d). The high-resolution TEM (HRTEM) image (Figure 1e) clearly demonstrates that the biomorphic  $\text{Mn}_3\text{O}_4$  was monocrystalline and derived from the lattice arrangement (inset of Figure 1e). The interplanar spacing was about 0.25 nm for the {211} lattice planes. The distribution of Mn (44.8 wt.%), C (31.7 wt.%), and O (23.5 wt.%) in the as-prepared sample was uniform (Figure 1f).

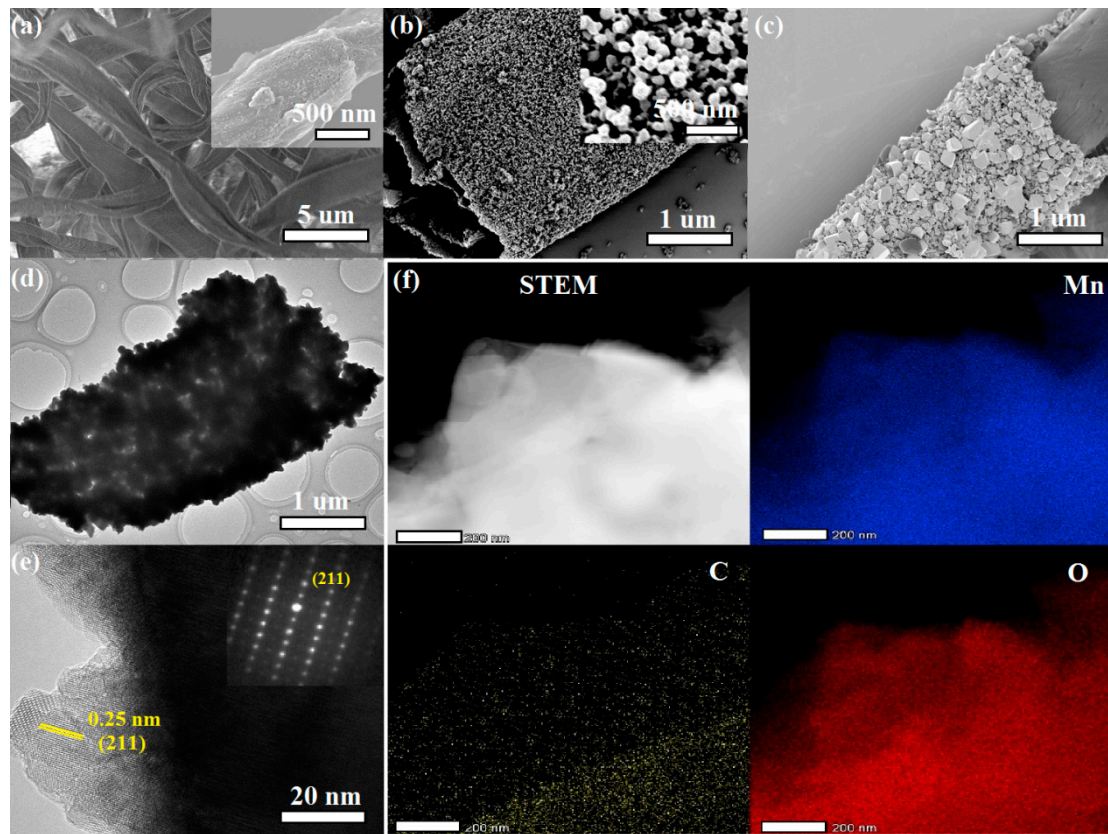


**Figure 1.** SEM images of (a) cotton and carbonized cotton fiber (inset in a); (b,c)  $\text{Mn}_3\text{O}_4$  nanocrystals grown on the PCM surface after 5 and 12 h, respectively. (d) Transmission electron microscopy (TEM) image, (e) high-resolution TEM (HRTEM) image (inset is the SEAD graph), and (f) energy dispersive spectroscopy (EDS) mappings of  $\text{Mn}_3\text{O}_4$ /PCM.

The XRD patterns of  $\text{Mn}_3\text{O}_4$ /PCM and bulk  $\text{Mn}_3\text{O}_4$  are shown in Figure 2a. The diffraction peaks of the composite can be ascribed to tetragonal  $\text{Mn}_3\text{O}_4$  (JCPDS 18-0803) [18], and the diffraction peak at  $25.24^\circ$  was ascribed to the carbon fabric (graphitic carbon: JCPDS75-1621), which was marked with an asterisk symbol (\*). Raman characterizations (Figure 2b) showed features from Mn–O in  $600\text{--}700\text{ cm}^{-1}$  and carbon fibers in the  $1200\text{--}1600\text{ cm}^{-1}$  region in  $\text{Mn}_3\text{O}_4$ /PCM [4,9,16], while only an Mn–O peak at lower wavenumber in  $\text{Mn}_3\text{O}_4$ .

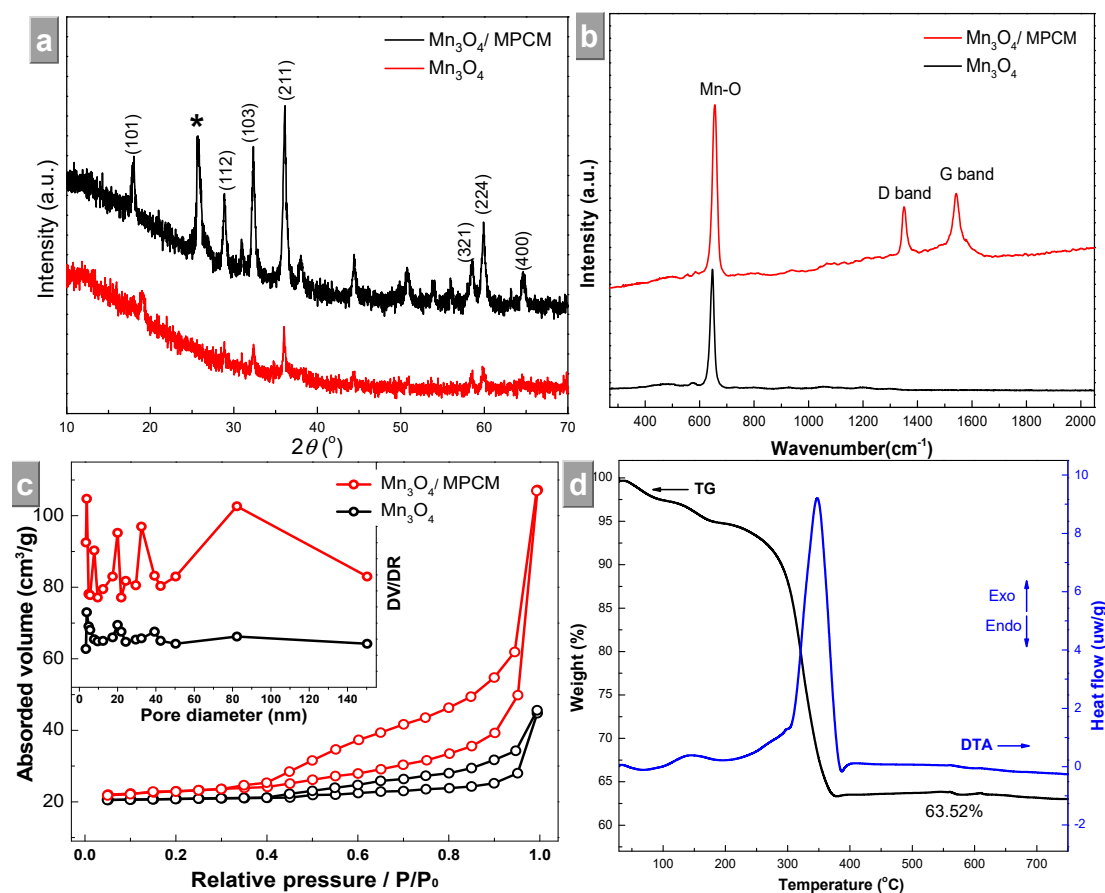


**Figure 2.** (a) XRD patterns, (b) Raman spectra, (c) nitrogen adsorption–desorption isotherms (inset shows pore size distributions) of  $\text{Mn}_3\text{O}_4/\text{PCM}$  and bulk  $\text{Mn}_3\text{O}_4$ , and (d) TG-DTA curves of the product.

The  $\text{N}_2$  adsorption–desorption isotherm of  $\text{Mn}_3\text{O}_4/\text{PCM}$  exhibited a distinct H3 hysteresis loop at  $p/p_0 > 0.40$  (Figure 2c). The isotherms of composite and pristine  $\text{Mn}_3\text{O}_4$  exhibited features of mesoporous materials. The pore size distribution of  $\text{Mn}_3\text{O}_4/\text{PCM}$  appeared with a wide range having two pore extremes at 24.2 and 82.5 nm. The BET specific surface area of the  $\text{Mn}_3\text{O}_4/\text{PCM}$  was determined to be  $51.9 \text{ m}^2 \cdot \text{g}^{-1}$ , which was much larger than that of pristine  $\text{Mn}_3\text{O}_4$  ( $10.8 \text{ m}^2 \cdot \text{g}^{-1}$ ). The higher surface area and pore volume is beneficial to the contact of the electrolytes with the active materials, and can further increase the electrochemical properties [6,8,10]. The TG-DTA curves of the hydrothermal product are shown in Figure 2d. Two endothermic peaks were observed in the range of 100–200 °C because of the adsorbed water. A weight loss of ~30% was found between 250 and 380 °C, which can be attributed to the decomposition of organic substances in cotton similar to other biomorphic oxides [13,14].

As shown in Figure 3a,b, the cyclic voltammetry (CV) and galvanostatic charge–discharge (GCD) curves of  $\text{Mn}_3\text{O}_4/\text{PCM}$  and bare  $\text{Mn}_3\text{O}_4$  demonstrated that the electrochemical properties of the former were better than those of the latter. The specific capacitances were calculated to be  $120.8$  and  $52.2 \text{ F} \cdot \text{g}^{-1}$ , respectively, which were attributed to the higher specific surface area of  $\text{Mn}_3\text{O}_4/\text{PCM}$ , the existence of carbon fiber, and its special hierarchical porous morphology derived from the biotemplate. As illustrated in Figure 3c,  $\text{Mn}_3\text{O}_4/\text{PCM}$  and pristine  $\text{Mn}_3\text{O}_4$  had a pair of redox peaks located at ~0.25 and ~0.4 V, which correspond to almost the same component and chemical conversion between different manganese oxidation states in alkaline medium ( $\text{Mn}_3\text{O}_4 \rightleftharpoons \text{MnOOH}$ ) [18,19]. The GCD curves of  $\text{Mn}_3\text{O}_4/\text{PCM}$  displayed remarkable pseudocapacitance properties. A slight reduction of specific capacitance was noted at high current densities (Figure 3d), indicating that the as-prepared composite has a good electrochemical stability [4,14].

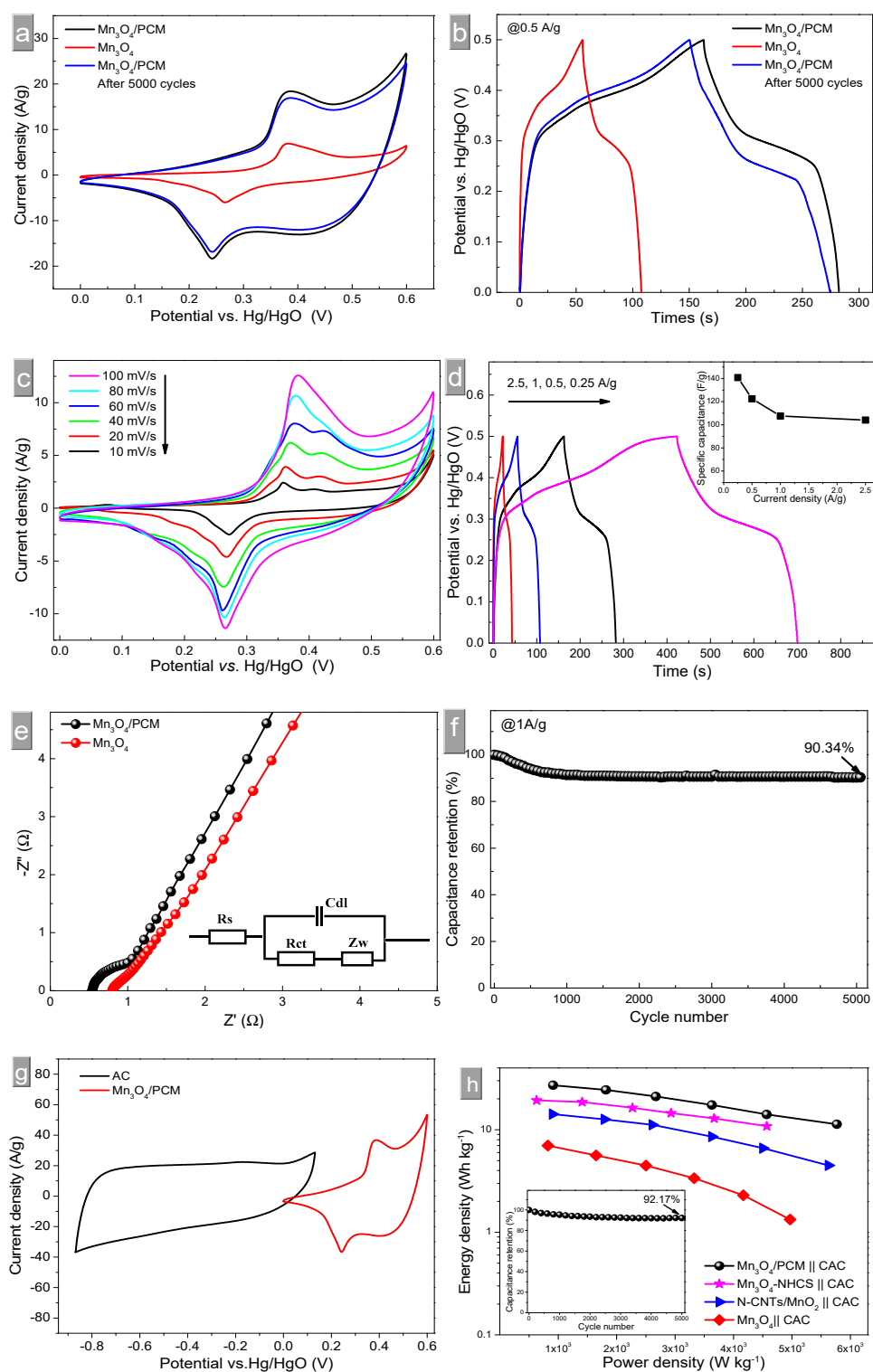


**Figure 3.** (a) Cyclic voltammetry (CV) curves at a scan rate of  $80 \text{ mV}\cdot\text{s}^{-1}$ ; (b) galvanostatic charge–discharge (GCD) curves at  $0.5 \text{ A}\cdot\text{g}^{-1}$  of  $\text{Mn}_3\text{O}_4/\text{PCM}$  and bare  $\text{Mn}_3\text{O}_4$ ; (c) CV curves of  $\text{Mn}_3\text{O}_4/\text{PCM}$  at various scan rates; (d) GCD curves and specific capacitance at various current densities of  $\text{Mn}_3\text{O}_4/\text{PCM}$  (inset in d); (e) Nyquist plots of  $\text{Mn}_3\text{O}_4/\text{PCM}$  and bare  $\text{Mn}_3\text{O}_4$ ; (f) capacitance retention of  $\text{Mn}_3\text{O}_4/\text{PCM}$  vs. cycle number at  $1 \text{ A}\cdot\text{g}^{-1}$ ; (g) CV curves of  $\text{Mn}_3\text{O}_4/\text{PCM}$  and CAC at  $20 \text{ mV}\cdot\text{s}^{-1}$ ; and (h) Ragone plots of asymmetrical supercapacitor in  $\text{MnO}_x$ -based two-electrodes systems. CAC: commercial active carbon.

The electrochemical impedance spectroscopy (EIS) measurements of the biomorphic  $\text{Mn}_3\text{O}_4/\text{PCM}$  and bulk  $\text{Mn}_3\text{O}_4$  are shown in Figure 3e. The charge-transfer resistance ( $R_{ct}$ ) (radius of the semicircle) of biomorphic electrode ( $\leq 0.5 \Omega$ ) was obviously lower than that of pristine  $\text{Mn}_3\text{O}_4$  ( $> 0.6 \Omega$ ), suggesting the substantially improved reaction kinetics (e.g., increased charge transfer rate) for microtubular  $\text{Mn}_3\text{O}_4/\text{PCM}$ . The increase in rate enables additional rapid redox reaction and facilitates electron transport, and thus improves the specific capacitance. As shown in Figure 3f, the long-term cycling stability of  $\text{Mn}_3\text{O}_4/\text{PCM}$  electrode was tested at  $1 \text{ A}\cdot\text{g}^{-1}$  for 5000 cycles. This result indicates that the electrode maintained more than 90% of its initial value after 5000 cycles, suggesting the excellent cyclic stability of the electrode. At the same time, the CV and GCD profiles after 5000 cycles migrated slightly from values before cycling (Figure 3a,b). The superior electrochemical performance of  $\text{Mn}_3\text{O}_4/\text{PCM}$  can be attributed to the special tubular morphology, high specific surface area, and porous carbon microfibers inside.

After assembling into an asymmetric supercapacitor using the two-electrode system of  $\text{Mn}_3\text{O}_4/\text{PCM}$  and CAC, the working voltage could be expanded to 0–1.4 V (Figure 3g) while the three-electrode system was 0–0.6 V. As shown in Figure 3h, the specific capacitance of  $\text{Mn}_3\text{O}_4/\text{PCM} \parallel \text{CAC}$  was  $110.8 \text{ F}\cdot\text{g}^{-1}$  at a current density of  $1 \text{ A}\cdot\text{g}^{-1}$ . The inset of Figure 3h is a Ragone plot of the asymmetric electrode. The energy density of the cell configuration was  $27.13 \text{ Wh}\cdot\text{kg}^{-1}$  at a power density of  $0.41 \text{ kW}\cdot\text{kg}^{-1}$ . Even at a high power density of  $4.76 \text{ kW}\cdot\text{kg}^{-1}$ , the energy density still maintained at  $11.34 \text{ Wh}\cdot\text{kg}^{-1}$ . Our results were better than previous reports concerned with special morphologies of  $\text{Mn}_3\text{O}_4$ -based composites used as supercapacity electrodes (Figure 3h) [4,20]. There was still specific capacitance of 92.17% retained in the cell after 5000 cycles (inset of Figure 3h), suggesting that the electrode has a high reversibility and good electrochemical stability.

#### 4. Conclusions

This work successfully prepared a biomorphic  $\text{Mn}_3\text{O}_4/\text{PCM}$  composite via a simple hydrothermal route by using cotton as a biotemplate. The as-obtained  $\text{Mn}_3\text{O}_4/\text{PCM}$  was composed of  $\text{Mn}_3\text{O}_4$  nanocrystal-coated carbon fiber, inherited the morphology and microstructure of cotton, and exhibited the excellent electrochemical properties of a specific capacitance of  $140.8 \text{ F}\cdot\text{g}^{-1}$  at  $0.25 \text{ A}\cdot\text{g}^{-1}$  and long cycling life with 90.34% of the capacitance after 5000 cycles. This work provides an example of the fabrication of biomorphic porous TMOs for developing promising electrode materials in energy storage and conversion.

**Author Contributions:** Original draft preparation, D.S.; review and editing, B.L.; literature search, L.H.; data collection, Y.L., J.L. and J.S.; data analysis, A.X.

**Funding:** This research was funded by the Natural Science Foundation of Fujian Province of China, grant number 2014H0028, Educational research projects for young and middle-aged teachers in Fujian Province, grant number JT180422, Program for the Innovative Research Team in Science and Technology in Fujian Province University, grant number 2018 and the Open Fund of open fund of Fujian Provincial Key Laboratory of Functional Materials and Applications (Xiamen University of Technology), grant number 608160030215.

**Conflicts of Interest:** The authors declare no conflict of interest. The funders had no role in the design of the study; in the collection, analyses, or interpretation of data; in the writing of the manuscript, or in the decision to publish the results.

#### References

1. Zhang, Y.Z.; Wang, Y.; Cheng, T.; Lai, W.Y.; Pang, H.; Huang, W. Flexible supercapacitors based on paper substrates: A new paradigm for low-cost energy storage. *Chem. Soc. Rev.* **2015**, *44*, 5181–5199. [[CrossRef](#)] [[PubMed](#)]
2. Li, B.; Dai, F.; Xiao, Q.; Yang, L.; Shen, J.; Zhang, C.; Cai, M. Nitrogen-doped activated carbon for high energy hybrid supercapacitor. *Energy Environ. Sci.* **2016**, *9*, 102–106. [[CrossRef](#)]
3. Huang, M.; Li, F.; Dong, F.; Zhang, Y.X.; Zhang, L.L.  $\text{MnO}_2$ -based nanostructures for high-performance supercapacitors. *J. Mater. Chem. A* **2015**, *3*, 21380–21423. [[CrossRef](#)]

4. Liu, T.; Jiang, C.; You, W.; Yu, J. Hierarchical porous C/MnO<sub>2</sub> composite hollow microspheres with enhanced supercapacitor performance. *J. Mater. Chem. A* **2017**, *5*, 8635–8643. [[CrossRef](#)]
5. Zang, J.; Ye, J.C.; Qian, H.; Lin, Y.; Zhang, X.W.; Zheng, M.S.; Dong, Q.F. Hollow carbon sphere with open pore encapsulated MnO<sub>2</sub> nanosheets as high-performance anode materials for lithium ion batteries. *Electrochim. Acta* **2018**, *260*, 783–788. [[CrossRef](#)]
6. Yan, D.L.; Li, S.C.; Zhu, G.S.; Wang, Z.M.; Xu, H.R.; Yu, A.B. Synthesis and pseudocapacitive behaviors of biomorphic mesoporous tubular MnO<sub>2</sub> templated from cotton. *Mater. Lett.* **2013**, *95*, 164–167. [[CrossRef](#)]
7. Zhou, Y.; Guo, L.; Shi, W.; Zou, X.F.; Xiang, B.; Xing, S.H. Rapid production of Mn<sub>3</sub>O<sub>4</sub>/rGO as an efficient electrode material for supercapacitor by flame plasma. *Materials* **2018**, *11*, 881. [[CrossRef](#)] [[PubMed](#)]
8. Aveiro, L.R.; Silva, A.G.M.D.; Antonin, V.S.; Candido, E.G.; Parreira, L.S.; Geonmonond, R.S.; Freitas, I.C.D.; Lanza, M.R.V.; Camargo, P.H.C.; Santos, M.C. Carbon-supported MnO<sub>2</sub> nanoflowers: Introducing oxygen vacancies for optimized volcano-type electrocatalytic activities towards H<sub>2</sub>O<sub>2</sub> generation. *Electrochim. Acta* **2018**, *268*, 101–110. [[CrossRef](#)]
9. Yan, D.L.; Zhang, H.; Chen, L.; Zhu, G.S.; Li, S.C.; Xu, H.R.; Yu, A.B. Biomorphic synthesis of mesoporous Co<sub>3</sub>O<sub>4</sub> microtubules and their pseudocapacitive performance. *ACS Appl. Mater. Interfaces* **2014**, *6*, 15632–15637. [[CrossRef](#)] [[PubMed](#)]
10. Wang, J.; Nie, P.; Ding, B.; Dong, S.; Hao, X.; Dou, H.; Zhang, X. Biomass derived carbon for energy storage devices. *J. Mater. Chem. A* **2016**, *5*, 2411–2428. [[CrossRef](#)]
11. Liu, Y.; Lv, B.; Liu, P.; Chen, Y.; Gao, B.; Lin, B. Biotemplate-assisted hydrothermal synthesis of tubular porous Co<sub>3</sub>O<sub>4</sub> with excellent charge-discharge cycle stability for supercapacitive electrodes. *Mater. Lett.* **2018**, *210*, 231–234. [[CrossRef](#)]
12. Cakici, M.; Kakarla, R.R.; Alonso-Marroquin, F. Advanced electrochemical energy storage supercapacitors based on the flexible carbon fiber fabric-coated with uniform coral-like MnO<sub>2</sub> structured electrodes. *Chem. Eng. J.* **2017**, *309*, 151–158. [[CrossRef](#)]
13. Sun, L.; Tian, C.G.; Li, M.T.; Meng, X.Y.; Wang, L.; Wang, R.H.; Yin, J.; Fu, H.G. From coconut shell to porous graphene-like nanosheets for high-power supercapacitors. *J. Mater. Chem. A* **2013**, *1*, 6462–6470. [[CrossRef](#)]
14. Saravanan, K.R.; Kalaiselvi, N. Nitrogen containing bio-carbon as a potential anode for lithium batteries. *Carbon* **2015**, *81*, 43–53. [[CrossRef](#)]
15. Tong, G.; Liu, Y.; Guan, J. In situ gas bubble-assisted one-step synthesis of polymorphic Co<sub>3</sub>O<sub>4</sub> nanostructures with improved electrochemical performance for lithium ion batteries. *J. Alloys Compd.* **2014**, *601*, 167–174. [[CrossRef](#)]
16. Sun, D.Y.; He, L.W.; Chen, R.Q.; Lin, Z.Y.; Lin, S.S.; Xiao, C.X.; Lin, B.Z. The synthesis, characterization and electrochemical performance of hollow sandwich microtubules composed of ultrathin Co<sub>3</sub>O<sub>4</sub> nanosheets and porous carbon by bio-template. *J. Mater. Chem. A* **2018**, *6*, 18987–18993. [[CrossRef](#)]
17. Sun, D.Y.; He, L.W.; Chen, R.Q.; Liu, Y.; Lv, B.J.; Lin, S.S.; Lin, B.Z. Biomorphic composites composed of octahedral Co<sub>3</sub>O<sub>4</sub> nanocrystals and mesoporous carbon microtubes templated from cotton for excellent supercapacitor electrodes. *Appl. Surf. Sci.* **2019**, *465*, 232–240. [[CrossRef](#)]
18. Wang, L.; Duan, G.R.; Chen, S.M.; Liu, X.H. Hydrothermally controlled synthesis of  $\alpha$ -MnO<sub>2</sub>,  $\gamma$ -MnOOH, and Mn<sub>3</sub>O<sub>4</sub> nanomaterials with enhanced electrochemical properties. *J. Alloys Compd.* **2018**, *752*, 123–132. [[CrossRef](#)]
19. Zhou, J.; Zhao, H.; Mu, X.; Chen, J.; Zhang, P.; Wang, Y.; He, Y.; Zhang, Z.; Pan, X.; Xie, E. Importance of polypyrrole in constructing 3D hierarchical carbon nanotube@MnO<sub>2</sub> perfect core-shell nanostructures for high-performance flexible supercapacitors. *Nanoscale* **2015**, *7*, 14697–14706. [[CrossRef](#)] [[PubMed](#)]
20. Zhu, J.; Xu, Y.; Hu, J.; Wei, L.; Liu, J.; Zheng, M. Facile synthesis of MnO<sub>2</sub> grown on nitrogen-doped carbon nanotubes for asymmetric supercapacitors with enhanced electrochemical performance. *J. Power Sources* **2018**, *393*, 135–144. [[CrossRef](#)]

